ACS SENSORS

pubs.acs.org/acssensors

Article

Lab-In-A-Syringe: A Novel Electrochemical Biosensor for On-Site and Real-Time Monitoring of Dopamine in Freely Behaving Mice

Amal Alachkar,* Sammy Alhassan, and Mehmet Senel*

Cite This: *ACS Sens.* 2022, 7, 331−337

Read Online

ACCESS | Metrics & More | Article Recommendations

ABSTRACT: There is a growing demand for real-time analysis and sampling of biofluids on a single low-cost platform in ultralow fluid volumes with robustness. In this study, a microfluidic sensor was developed, manufactured through an additive manufacturing technique, and used for dopamine (DA) measurements. We implemented a biosensing system using pencil graphites (PGEs) integrated into a three-dimensional (3D) printed microfluidic syringe-type device (μSyringe). The amperometry technique was used to monitor the current changes associated with the electrooxidation of DA. The sensing signal was stable and linear in a concentration range of DA between the limit of quantification (0.1 nM) and the upper limit of linearity (500 nM). The μSyringe sensing device is simple, robust, and stable, making it suitable for real-time measurement of DA in cerebrospinal fluid (CSF) from freely moving mice.

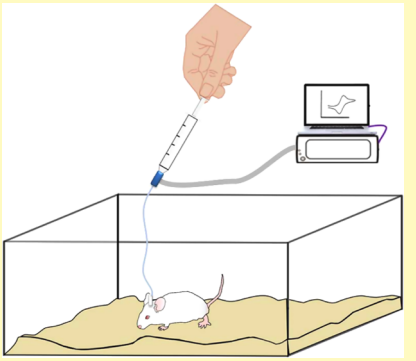

KEYWORDS: *electrochemical sensor, dopamine, graphite electrode, fluidic sensor, 3D printing*

Downloaded via TSINGHUA UNIV on November 13, 2022 at 02:31:02 (UTC).
See https://pubs.acs.org/sharingguidelines for options on how to legitimately share published articles.

Microfluidic analysis systems (μFAS) have typical flow rates of nL to μL min^{-1} due to their micrometer diameter of the flow channels.[1] Also, their small structure allows fabricating a single device to perform several analytical standard processes required on conventional flow analysis systems.[2] However, sampling is a major difficulty of using μFAS due to the requirement of micropumps or external pumps, which are expensive and challenging to integrate microfluidic channels. To resolve this challenge, self-pumping or sampling microfluidics has been developed.[3] In recent years, great attention has been given to the construction of microflow systems using an additive manufacturing approach.[4]

Dopamine (DA) is a major neurotransmitter that plays crucial roles in several physiological functions, including controlling movement and regulating emotions and cognitive functions. Moreover, perturbed dopamine systems and abnormal dopamine levels are associated with neurological and psychiatric disorders such as Parkinson's disease, Huntington's disease, depression, schizophrenia, attention deficiency and hyperactivity disorder (ADHD), Tourette symptoms, and drug addiction.[5,6] Therefore, monitoring dopamine levels related to its multiple functions in the brain or associated with pathological conditions has been essential for understanding dopamine roles in neural processes in the brain.[7,8] Furthermore, dopamine levels in different brain regions are dynamic, and changes in the dopamine concentration might be momentary in response to environmental stimuli and drug administration. Consequently, developing tools for real-time monitoring of dopamine in freely behaving animals is crucial to correlate dopamine level fluctuations with specific behavioral activities. Several techniques and assays have been designed for detecting dopamine and monitoring its fluctuations and dynamics, including electrochemical, optical, magnetic, microdialysis, cell-based fluorescent engineered receptor, and gene expression-based assays.[6−12] However, most of these technologies have limitations. For instance, while some techniques provide high-resolution measurements of dopamine, they can only allow a single-point evaluation of samples. On the other hand, other methods can give direct and real-time measurements of dopamine, however, with low sensitivity. Therefore, there is a strong demand for devices and techniques that can monitor in vivo real-time dopamine concentration changes in animal behavior, with high specificity and high sensitivity in the physiological range.

In this study, we describe the development of a low-volume and fluidic sensing device for instantaneous detection of dopamine in biological fluids in real-time in freely behaving mice. Moreover, this work reports, for the first time, the syringe-type sensing device for biofluid sampling and analysis.

Received: November 30, 2021
Accepted: December 31, 2021
Published: January 10, 2022

© 2022 American Chemical Society

https://doi.org/10.1021/acssensors.1c02525
ACS Sens. 2022, 7, 331−337

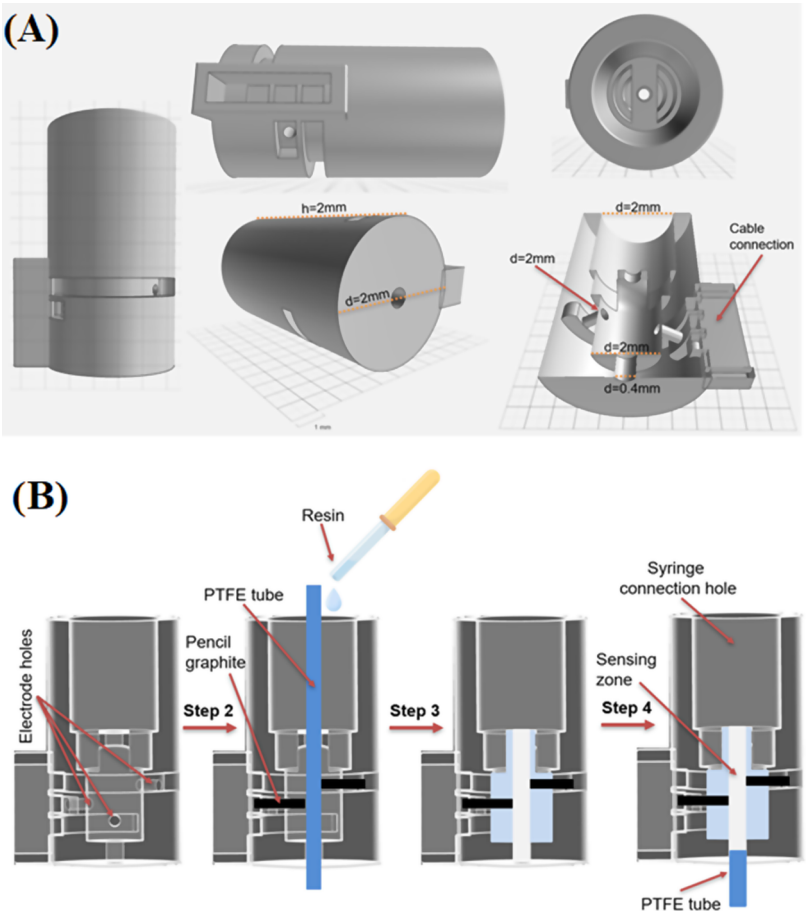

Figure 1. (A) Three-dimensional (3D) model of the μSyringe sensing device used during the DA measurements with the positions of the electrodes. Schemes showing the layout of sensing electrodes and fluidic channels and details about the geometry of μSyringe. (B) Scheme of μSyringe sensor fabrication (insertion of PGEs in the cavities on the 3D-printed holder; curing resin and attaching the sampling tube) and image of the μSyringe.

The sample volume is the lowest (0.54 μL) in the literature among the additive manufactured sensing devices.

EXPERIMENTAL SECTION

Materials. Dopamine, glucose (Gl), Nafion, uric acid (UA), ascorbic acid (AA), sodium chloride, and potassium chloride were purchased from Sigma-Aldrich. Human serum was used as a real sample and was obtained from Sigma-Aldrich. All chemicals were of analytical grade and were used without further purification, and all solutions were prepared with double-distilled water (ddH_2O) unless stated otherwise.

Syringe Sensor Fabrication. The μSyringe was fabricated, as shown in Figure 1. The fabrication process of the μSyringe consisted of three consequent steps. First, μSyringe was designed using SolidWorks software (Dassault Systemes, France) with a typical plan, as shown in Figure 1A. The inner diameter of the sensing channel of the device was 400 μm, and the inner electroactive sensor volume was calculated as ∼0.54 μL. The respective file in .STL format was then opened with Anycubic Photon 3D SLA printer software (downloaded free from Anycubic website) to determine the printing conditions (layer thickness: 0.03 mm, with an exposure time of 8 s, off time of 1 s, and printing speed of 3 mm/s). In the second step, microfluidic devices were printed using a high-resolution SLA 3D printer (Anycubic, China) featuring a 51 μm XY resolution and a 130 × 78 × 160 (h) mm printing area. The file (sliced drawing) was saved on a memory card inserted in the printer, and the printing process was initiated with a UV wavelength of 358−405 nm. The UV light was projected from the bottom of the resin bath (filled with Anycubic transparent resin 405). After printing, the microfluidic device was removed from the building platform with forceps, followed by a washing step of the uncured resin with ethanol. Afterward, the microchannel was exposed to a UV light with 405 ± 5 nm wavelength within a curing chamber for the postcuring process. The image of the three-dimensional (3D)-printed device is shown in Figure 1B. Finally, three flat-shaped pencil graphites (PGEs) were inserted into special cavities on the 3D-printed flow device. Next, a hole was opened in the middle of the flat surface of the flow device using a manual drilling machine (diameter: 400 μm). Eventually, tubes (Cole-Parmer, Masterflex Transfer Tubing, Teflon [poly(tetrafluoroethylene), PTFE] 305 μm inner diameter, and 402 μm outer diameter) were connected to the microchannel by a tweezer and sealed with epoxy resin.

Electrochemical Measurements. All electrochemical measurements were carried out using a CompactStat portable electrochemical potentiostat (Ivium Technologies). PGEs were used as working, counter, and reference electrodes and connected to the potentiostat with crocodile clips. The Nafion solution in ethanol (2% w/w) was flowed in the μSyringe and left to dry for 10 min in the obtained selective sensing electrode. The PGEs in the μSyringe were activated electrochemically by cyclic voltammetry (CV) scanning at a positive potential between 0 and 1.2 V with a scan rate of 100 mV/s for 50 cycles in a 0.1 M phosphate buffer solution (pH 7.4). Amperometric current−time plots were obtained by three successive analyses of a DA solution prepared in 10 mM pH 7.4 phosphate-buffered saline (PBS) under a fixed operating potential of +200 mV.

Animal Study. All experimental procedures were approved by the Institutional Animal Care and Use Committee of the University of

https://doi.org/10.1021/acssensors.1c02525
ACS Sens. 2022, 7, 331−337

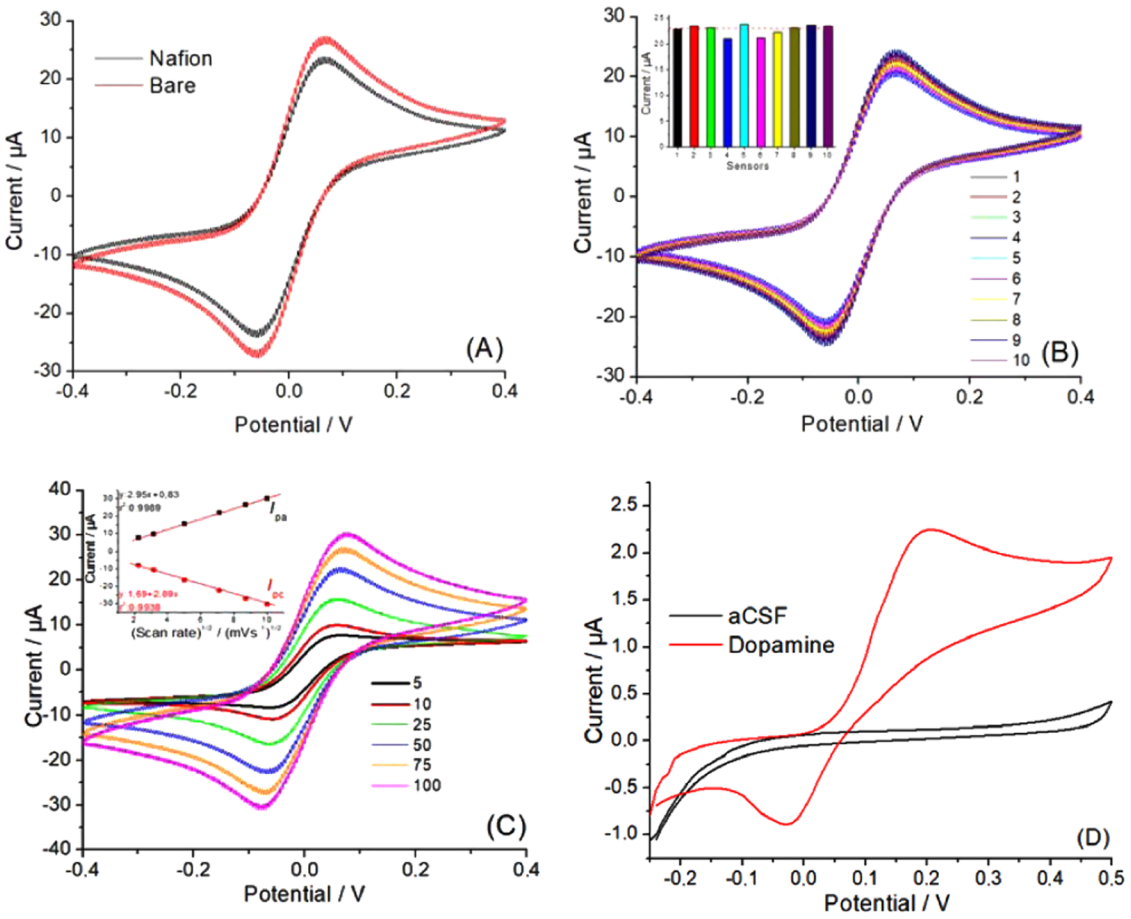

Figure 2. Electrochemical characterization measurements performed in the 5 mM $K_4Fe(CN)_6/K_3Fe(CN)_6$ (1:1 ratio) solution containing 0.1 M KCl. (A) CV scan of the μSyringe recorded at 50 m/(V s). (B) CV plots were obtained from 10 different μSyringe sensing electrodes with the inset graph showing each electrode's oxidation peak current value. (C) Effect of the change in the scan rate from 5 to 100 m/(V s) on the current response of the μSyringe with the inset graph showing current versus square root of scan rate potential. (D) CV plots of the μSyringe sensing device in the absence of DA when using artificial cerebrospinal fluid (aCSF) (black line) and 500 nM DA recorded in aCSF (red line).

California, Irvine, and were performed in compliance with national and institutional guidelines for the care and use of laboratory animals.

Monitoring the DA Content in the Mouse CSF. *Animals and Stereotaxic Surgery: Cannulation for Sampling of CSF from Intracerebroventricles (ICVs).* Stereotaxic surgery was carried out on 8 week old Swiss Webster male mice ($n = 5$) to implant a stainless-steel guide cannula into the lateral ventricles (20 gauge guide cannulas with 2.5 mm custom-cut depth, PlasticsOne) (Figure 2A). Animals were anesthetized with 2% isoflurane anesthesia (Institutional Animal Care and Use Committee guidelines). Animals were then secured in a Kopf stereotaxic instrument. A guide cannula was implanted at −0.22 mm posterior to bregma, 1.0 mm lateral, and 2.3 mm below the skull surface.[13] Dental acrylic cement was used to fasten the cannula to the skull, and caps were inserted into the cannulas. Animals were allowed to recover for 1 week.

To determine the kinetics of amphetamine-induced increase in locomotor activity, mice not subjected to cannulation were used for the behavioral study. On the experiment day, four animals were injected intraperitoneally (IP) with amphetamine (1 mg/kg), and the control group (4 animals) were injected with saline (10 μL/gr). Animals' locomotor activities were monitored as described previously.[14] Briefly, mice were placed into 40 × 40 cm^2 locomotion test chambers (Med Associates, Fairfax, VT) and allowed to habituate for 30 min before the test. The locomotor activities were recorded for 4 h and analyzed using Activity Monitor 5 software (Med Associates).

Since the peak effect of amphetamine occurred 30 min and was diminished at 2 h after injection, we collected the CSF samples from the lateral ventricle of a new group of mice subjected to cannulation at three time points: 0, 30, and 120 min after injection of amphetamine 1 mg/kg.

RESULTS AND DISCUSSION

Electrochemical Characteristics. Cyclic voltammetry is employed to characterize the electrochemical performances of bare PG and Nafion-coated PG electrodes in the μSyringe for the fabrication of dopamine biosensors. Figure 2A shows the CV obtained at bare PGE and Nafion-coated PGE at a scan rate of 50 mV/s in a 5 mM $K_4Fe(CN)_6/K_3Fe(CN)_6$ (1:1 ratio) solution containing 0.1 M KCl. It was observed that the current corresponding to the oxidation at the bare PG electrode (27 μA) is higher as compared to that of the Nafion-coated PG electrode (23 μA), confirming the successful coating of Nafion on the PGE surface in the μSyringe.

The reproducibility of the process implemented to fabricate the μSyringe sensing device was investigated using 10 randomly selected μSyringe sensing electrodes. Figure 2B shows the CV plot of the μSyringe sensors recorded in a ferri-ferrocyanide solution with a scan rate of 50 mV/s, where well-defined oxidation−reduction peaks for all electrodes were observed. The inset of Figure 2B shows the comparison of the current peak values of 10 different randomly selected μSyringe sensing electrodes with a current peak value of 22.48 ± 1.56 μA (6.3% standard deviation). These results showed that the

https://doi.org/10.1021/acssensors.1c02525
ACS Sens. 2022, 7, 331−337

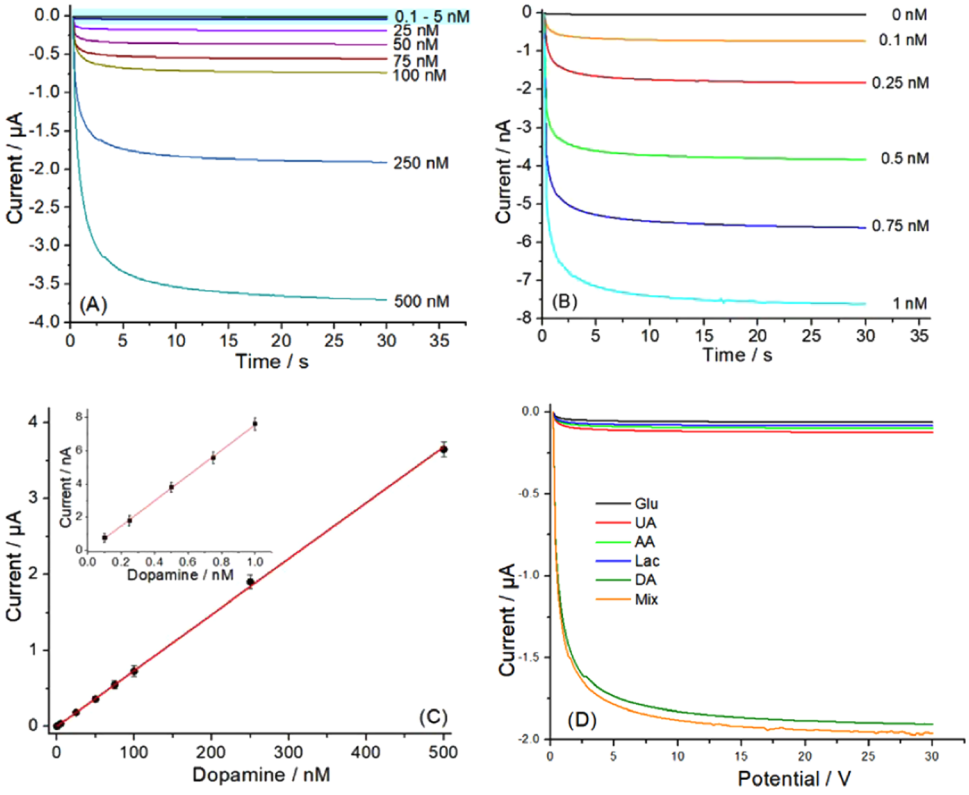

Figure 3. Characterization of the microsensing device responses. (A) Complete amperometric curve graphs obtained with DA concentrations ranging from 0.1 to 500 nM. (B) Amperometric plot of the lower DA concentrations as zoomed-in parts of the previous plots. (C) Calibration plot obtained with an inset showing the DA concentration. Error bars show the standard deviation of three data sets. (D) Selectivity testing of the μSyringe sensing device using 5 mM glucose (Gl), 5 mM lactate (La), 20 μM uric acid (UA), or 20 μM ascorbic acid (AA), and as a positive control 500 nM DA or mixed solution composed of all aforementioned tested interferons with DA at the indicated concentrations.

Table 1. Comparison of the Performance Characteristics of Various Electrochemical Methods for DA Sensors with Proposed Electrodes[a]

electrode material	detection technique	linear range (μM)	detection limit (nM)	sensitivity (μA μM^{-1})	working volume (μL)	real sample	ref
PG	amp.	0.0001−0.5	0.1	3.53 ± 0.08	0.54	mouse CSF	this work
Au μE	amp.	0.0001−1	0.1	3.53 ± 0.08	2.40	mouse CSF and plasma	15
SPCE/HPC/pTBA-EB	CV	0.00005−0.13	0.034	0.035	NR	human blood plasma	16
Gn/Gt/Ch/PEG	DPV	0.5−120	10	0.62	30	urine and blood	17
MWCNT-CPE/PDDA-RGO	DPV	0.05−120	16	0.0041	20	rat plasma	18
Pt μEA	amp.	0−80	5000	NR	5	spheroid-released DA	19
CNP/ITO	SWV	0.010−0.5	3.5	NR	40	human serum	20
SWCNT/Au	amp.	0.025−1	0.05	0.0078	50		21

[a]DPV: differential pulse voltammetry, Amp: amperometry, PG: pencil graphite, ITO: indium-tin-oxide, Gn/Gt/Ch/PEG: graphene/graphite/chitosan/poly(ethylene glycol), CNP/ITO: ITO functionalized with carbon nanoparticles, NR: not reported, SWCNT/Au: Au electrode coated with single-walled carbon nanotubes, MWCNT-CPE/PDDA-RGO: multiwalled carbon nanotube containing a carbon paste electrode later on modified with poly (diallyl dimethylammonium) and reduced graphene oxide, CNP: cerium nanoparticle, NPS: nanostructured plasmonic substrate, LSPR: localized surface plasmonic resonance, CFμE: carbon-fiber microelectrode, SPCE/HPC/pTBA-EB: screen-printed carbon electrode modified with N, S-doped porous carbon and poly(2,2:5,5-terthiophene-3-*p*-benzoic acid) and Evans blue, and AuNP: Au nanoparticle.

μSyringe sensors' fabrication process is highly reproducible, and we could generate μSyringe sensors with almost identical electrochemical properties.

The effect of different scan rates on the cyclic voltammograms of the PG electrode in a 5 mM $K_4Fe(CN)_6/K_3Fe(CN)_6$ (1:1 ratio) solution containing 0.1 M KCl was investigated, as shown in Figure 2C. It can be seen that with the increase of the scan rate (10−100 mV/s), the redox peak currents of ferrocyanide increase (inset of Figure 2C). The equation of $I = (-2.29 \pm 3.47) + (1.65 \pm 0.05)\nu$ ($R^2 = 0.9993$) indicates the linear relationship between the oxidation peak current of ferrocyanide and scan rate (ν). It was obvious that the electrochemical oxidation reaction of ferrocyanide is an adsorption-controlled process.

To further investigate the electrochemical oxidation of DA, the cyclic voltammogram of the μSyringe sensing electrode at a

https://doi.org/10.1021/acssensors.1c02525
ACS Sens. 2022, 7, 331−337

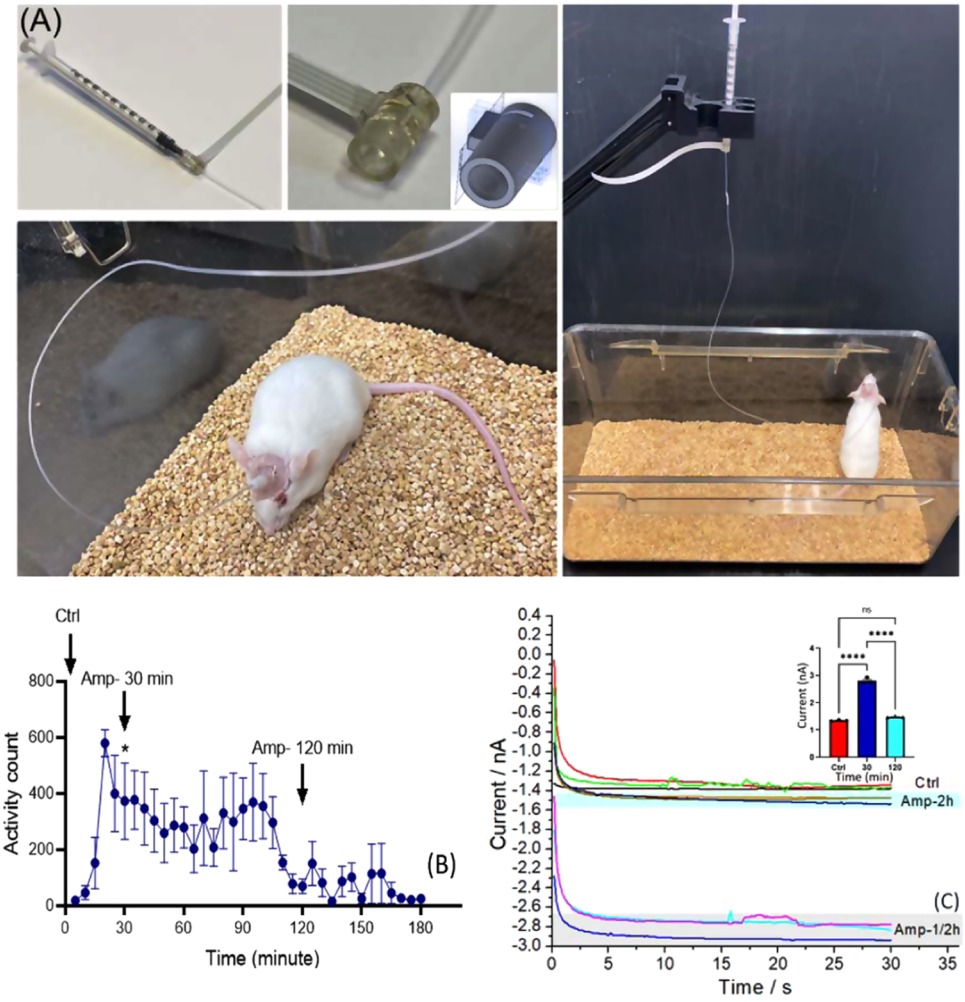

Figure 4. μSyringe sensing device use in monitoring CSF DA concentrations in freely moving mice. (A) Overview schematic of the experimental setting showing the μSyringe sensing device and its sampling tube inserted into a mouse brain for CSF extraction. (B) Locomotor activity counts induced by amphetamine (amphetamine was injected at time 0 min); arrows indicate the time points at which CSF samples were taken; *P = 0.018, compared to the control condition, one-way analysis of variance (ANOVA), followed by the Tukey post-test; (C) DA concentration measured, using the μSyringe sensing device, in the CSF of amphetamine-treated mice at different time points; ****P <0.0001, one-way ANOVA, followed by the Tukey post-test.

scan rate of 50 mV/s in aCSF and aCSF at pH 7.4 including 500 nM DA is exhibited in Figure 4D. The anodic and cathodic peak potentials of the DA on the surface of the PG electrode were observed at 0.2 and −0.025 V, respectively. On the other hand, there was no response observed in aCSF. These results show that the μSyringe sensing electrode has high electrocatalytic performances for the electrochemical oxidation and reduction of DA. Therefore, the oxidation peak potential of DA is located at ∼0.2 V.

Sensing Performance of the μSyringe Sensing Device. *Amperometric Measurement of Dopamine.* Fabrication of low-cost and scalable wearable and point-of-care biosensors is important healthcare technology. To demonstrate the potential of additive manufacturing tools for the fabrication of low-volume microfluidic devices, we used an SLA-based 3D printer and pencil graphites. As shown in Figure 1, the fabrication of an ultralow-volume 3D-printed microsyringe sensing device was achieved in a three-step process. The resulting microsensing device responses are shown in Figure 3. The amperometric response kinetics of the μSyringe sensing device was characterized at an increasing concentration of dopamine (0.1−500 nM) in the artificial cerebrospinal fluid (aCSF), as shown in Figure 3A,B. Figure 3A−C shows that the peak currents of the amperometric response of DA were linearly related to its concentrations. The μSyringe sensing device responded very quickly and reached a steady state within 5−10 s. A linear dynamic range of 0.1 nM to 0.5 μM with a linear correlation coefficient of 0.9991 and a calculated limit of detection of 0.62 nM DA was observed (the linear equation was Ip(μA) = 0.008C (mM) + 1.53 × 10^{-5}). DA response was linear in the concentration range of 0.1−1 nM with a detection limit of 0.1 nM was calculated based on S/N of 3, and the linear equation was Ip(μA) = 2C (mM) + 6.18, with the linear correlation coefficient R^2 of 0.9993.

Table 1 presents a comparison of the analytical parameters of the biosensors fabricated by our group to other sensors and biosensors in the literature. The analytical parameters of our μSyringe sensing device, including dynamic range and sensitivity, were comparable with values reported earlier by other research groups. These results demonstrate that our fabrication approach is suitable to fabricate an ultralow-volume fluidics sensing device for point-of-care applications and that its syringe design is useful for real-time on-site measurements.

https://doi.org/10.1021/acssensors.1c02525
ACS Sens. 2022, 7, 331−337

Since dopamine generally coexists with the other molecules in the CSF, including the AA, UA, glucose, and protein, it is essential to confirm the selectivity of the developed electrode toward dopamine detection. The interference mitigation capability of the μSyringe for the detection of DA in the presence of various compounds [5 mM glucose (Gl), 5 mM lactate (La), 20 μM uric acid (UA), or 20 μM ascorbic acid (AA), and as a positive control 500 nM DA] was investigated using amperometric analysis. The results in Figure 3D show no significant changes in the peak currents for the above-mentioned interferent compounds. It is evident that AA, Lac, Glu, and UA show almost negligible interference in detecting DA, therefore, showing no significant effects of interferences from other compounds. These findings demonstrate that the developed platform, μSyringe sensor electrode, is a powerful tool for the electrochemical detection of dopamine, one of the most important neurotransmitters, in terms of sensitivity and selectivity.

Real Sample Analysis. To investigate its capability to analyze real-time samples, the μSyringe sensing device was employed to monitor CSF DA concentrations in freely moving mice that have been treated with amphetamine, a dopamine releasing agent that is known to cause locomotor hyperactivity. Locomotor activity is known to be correlated with the levels of dopamine in the brain. The μSyringe sensing device with a PTFE tube fixed on a stand and the end of the tube was inserted and fixed into the mouse brain with a cannula, as shown in Figure 4. CSF samples were analyzed at three different time points that correspond to different levels of amphetamine-induced locomotor activity. The results show that at 30 min after amphetamine injection, mice exhibited hyperactivity ($F_{(2,15)}$ = 5.714, P = 0.018, compared to the control condition at 0 min time point, one-way ANOVA, followed by the Tukey post-test, Figure 4B). Alongside the hyperactivity at 30 min, there was a significant increase in dopamine levels as measured by our μSyringe sensing device ($F_{(2,6)}$ = 508.9, P <0.0001, one-way ANOVA, followed by the Tukey post-test, Figure 4C). At 120 min, the effect of amphetamine dramatically decreased and the locomotor activity returned to the control levels (P > 0.05, compared to the control condition, one-way ANOVA, followed by the Tukey post-test, Figure 4B). In parallel, CSF dopamine levels were decreased to levels comparable with those in the control condition (P = 0.086, one-way ANOVA, followed by the Tukey post-test, Figure 4C). These results indicate the accuracy of the biosensor in determining the DA content in real samples.

CONCLUSIONS

In summary, we have demonstrated the development and functionality of a novel, simple, and ultralow-volume biomarker detection device suitable for on-site point-of-care applications. The results indicated that our μSyringe sensing device could measure the concentration of DA in its physiologically relevant ranges in CSF from freely moving animals without consuming a sample. Further development of the design will make the device capable of simultaneously measuring multibiomarkers, with attention to the added challenges of working in complex sample matrices.

AUTHOR INFORMATION

Corresponding Authors

Amal Alachkar − *Department of Pharmaceutical Sciences, University of California, Irvine, California 92697-4625, United States; Institute for Genomics and Bioinformatics, School of Information and Computer Sciences and Center for the Neurobiology of Learning and Memory, University of California-Irvine, Irvine, California 92697-4625, United States;* orcid.org/0000-0002-5365-1726; Email: aalachka@uci.edu

Mehmet Senel − *Department of Pharmaceutical Sciences, University of California, Irvine, California 92697-4625, United States; Department of Biochemistry, Faculty of Pharmacy, Biruni University, Istanbul 34010, Turkey;* orcid.org/0000-0001-7366-4746; Email: msenel@uci.edu, msenel@biruni.edu.tr

Author

Sammy Alhassan − *Department of Pharmaceutical Sciences, University of California, Irvine, California 92697-4625, United States*

Complete contact information is available at: https://pubs.acs.org/10.1021/acssensors.1c02525

Notes

The authors declare no competing financial interest.

REFERENCES

(1) Agustini, D.; Bergamini, M. F.; Marcolino-Junior, L. H. Characterization and optimization of low cost microfluidic thread based electroanalytical device for micro flow injection analysis. *Anal. Chim. Acta* **2017**, *951*, 8−115.

(2) Miró, M.; Hansen, E. H. Miniaturization of environmental chemical assays in flowing systems: The lab-on-a-valve approach vis-à-vis lab-on-a-chip microfluidic devices. *Anal. Chim. Acta* **2007**, *600*, 46−57.

(3) Kokalj, T.; Park, Y.; Vencelj, M.; Jenkoa, M.; Lee, L. P. Self-powered Imbibing Microfluidic Pump by Liquid Encapsulation: SIMPLE. *Lab Chip* **2014**, *14*, 4329−4333.

(4) Senel, M.; Alachkar, A. Lab-in-a-pencil graphite: A 3D-printed microfluidic sensing platform for real-time measurement of anti-psychotic clozapine level. *Lab Chip* **2021**, *21*, 405−411.

(5) Klein, M. O.; Battagello, D. S.; Cardoso, A. R.; Hauser, D. N.; Bittencourt, J. C.; Correa, R. G. Dopamine: functions, signaling, and association with neurological diseases. *Cell. Mol. Neurobiol.* **2019**, *39*, 31−59.

(6) Tidey, J. W.; Miczek, K. A. Social defeat stress selectively alters mesocorticolimbic dopamine release: an in vivo microdialysis study. *Brain Res.* **1996**, *721*, 140−149.

(7) Robinson, D. L.; Venton, B. J.; Heien, M. L.; Wightman, R. M. Detecting subsecond dopamine release with fast-scan cyclic voltammetry in vivo. *Clin. Chem.* **2003**, *49*, 1763−1773.

(8) Muller, A.; Joseph, V.; Slesinger, P. A.; Kleinfeld, D. Cell-based reporters reveal in vivo dynamics of dopamine and norepinephrine release in murine cortex. *Nat. Methods* **2014**, *11*, 1245−1252.

(9) Inagaki, H. K.; Ben-Tabou de-Leon, S.; Wong, A. M.; Jagadish, S.; Ishimoto, H.; Barnea, G.; Kitamoto, T.; Axel, R.; Anderson, D. J. Visualizing neuromodulation in vivo: TANGO-mapping of dopamine signaling reveals appetite control of sugar sensing. *Cell* **2012**, *148*, 583−595.

(10) Lee, D.; Creed, M.; Jung, K.; Stefanelli, T.; Wendler, D. J.; Oh, W. C.; Mignocchi, N. L.; Lüscher, C.; Kwon, H. Temporally precise labeling and control of neuromodulatory circuits in the mammalian brain. *Nat. Methods* **2017**, *14*, 495−503.

(11) Kruss, S.; Salem, D.; Vuković, L.; Lima, B.; Ende, E. V.; Boyden, E. S.; Strano, M. S. High-resolution imaging of cellular

dopamine efflux using a fluorescent nanosensor array. *Proc. Natl. Acad. Sci. U.S.A.* **2017**, *114*, 1789−1794.
(12) Beyene, A. G.; Delevich, K.; Del Bonis-O'Donnell, J. T.; Piekarski, D. J.; Lin, W. C.; Thomas, A. W.; Yang, S. J.; Kosillo, P.; Yang, D.; Prounis, G. S.; Wilbrecht, L.; et al. Imaging striatal dopamine release using a nongenetically encoded near infrared fluorescent catecholamine nanosensor. *Sci. Adv.* **2019**, *5*, No. eaaw3108.
(13) Paxinos, G.; Franklin, K. B. *The Mouse Brain in Stereotaxic Coordinates*; Academic Press, 2001.
(14) Wang, L.; Zhang, Y.; Wang, C.; Zhang, X.; Wang, Z.; Liang, X.; Alachkar, A.; Civelli, O. A Natural Product with High Affinity to Sigma and 5-HT 7 Receptors as Novel Therapeutic Drug for Negative and Cognitive Symptoms of Schizophrenia. *Neurochem. Res.* **2019**, *44*, 2536−2545.
(15) Senel, A.; Dervisevic, E.; Alhassen, S.; Dervisevic, M.; Alachkar, A.; Cadarso, V. J.; Voelcker, N. H. Microfluidic Electrochemical Sensor for Cerebrospinal Fluid and Blood Dopamine Detection in a Mouse Model of Parkinson's Disease. *Anal. Chem.* **2020**, *92*, 12347−12355.
(16) Seo, K.-D.; Hossain, M. M. D.; Gurudatt, N. G.; Choi, C. S.; Shiddiky, M. J. A.; Park, D.-S.; Shim, Y.-B. Microfluidic neurotransmitters sensor in blood plasma with mediator-immobilized conducting polymer/N, S-doped porous carbon composite. *Sens. Actuators, B* **2020**, No. 128017.
(17) Manbohi, A.; Ahmadi, S. H. Sensitive and selective detection of dopamine using electrochemical microfluidic paper-based analytical nanosensor. *Sens. Bio-Sens. Res.* **2019**, *23*, No. 100270.
(18) Liu, Z.; Jin, M.; Cao, J.; Niu, R.; Li, P.; Zhou, G.; Yu, Y.; van den Berg, A.; Shui, L. Electrochemical sensor integrated microfluidic device for sensitive and simultaneous quantification of dopamine and 5-hydroxytryptamine. *Sens. Actuators, B* **2018**, *273*, 873−883.
(19) Abe, H.; Ino, K.; Li, C.-Z.; Kanno, Y.; Inoue, K. Y.; Suda, A.; Kunikata, R.; Matsudaira, M.; Takahashi, Y.; Shiku, H.; Matsue, T. Electrochemical Imaging of Dopamine Release from Three-Dimensional-Cultured PC12 Cells Using Large-Scale Integration-Based Amperometric Sensors. *Anal. Chem.* **2015**, *87*, 6364−6370.
(20) Rozniecka, E.; Jonsson-Niedziolka, M.; Celebanska, A.; Niedziolka-Jonsson, J.; Opallo, M. Electrochemical Detection of Dopamine and Serotonin in the Presence of Interferences in a Rotating Droplet System. *Analyst* **2014**, *139*, 2896−2903.
(21) Sansuk, S.; Bitziou, E.; Joseph, M. B.; Covington, J. A.; Boutelle, M. G.; Unwin, P. R.; Macpherson, J. V. Ultrasensitive Detection of Dopamine Using a Carbon Nanotube Network Microfluidic Flow Electrode. *Anal. Chem.* **2013**, *85*, 163−169.

Recommended by ACS

Electrochemical Carbamazepine Aptasensor for Therapeutic Drug Monitoring at the Point of Care
Saeromi Chung, Drew A. Hall, *et al.*
OCTOBER 17, 2022
ACS OMEGA
READ

Reversible Immunosensor for the Continuous Monitoring of Cortisol in Blood Plasma Sampled with Microdialysis
Laura van Smeden, Menno W. J. Prins, *et al.*
OCTOBER 18, 2022
ACS SENSORS
READ

In Vivo Chemogenetic Biocompatibility of Mercury as a Specific Hypercalcemia Actuator in Snail's Spinal Cord Cell Manipulation: An Extracellular Field Potential Biosensor
Sajedeh Karami, Amir Mootabi-Alavi, *et al.*
JULY 13, 2022
ACS APPLIED BIO MATERIALS
READ

Optimized Sawhorse Waveform for the Measurement of Oxytocin Release in Zebrafish
Romana Jarosova, Michael A. Johnson, *et al.*
FEBRUARY 02, 2022
ANALYTICAL CHEMISTRY
READ

Get More Suggestions >

https://doi.org/10.1021/acssensors.1c02525
ACS Sens. 2022, 7, 331−337